The role of ionization in symbiotic binaries

Augustin Skopal
Astronomical Institute, Slovak Academy of Sciences, SK-059 60 Tatranská Lomnica, Slovakia

Abstract

Processes of ionization and recombination often influence significantly the observed spectrum produced by symbiotic stars in a very wide wavelength region. Properties of the nebular spectrum provide important information on some fundamental parameters and on geometric structure of symbiotic stars. This paper reviews the recently recognized effects of ionization/recombination in these binaries and summarizes first results. We concentrate in this review on the continuum emission in the range from ultraviolet to near-IR wavelengths.

1 Introduction

The objects, which are now commonly named as *symbiotic stars* were discovered at the beginning of the 20th century as stars with peculiar and/or combined spectra [13,30], because of the simultaneous presence of spectral features indicating two very distinct temperature regimes. Their present denotation was used for the first time by [29]. Currently the symbiotic stars are understood as interacting binary systems consisting of a cool giant and a hot compact star, which is in most cases a white dwarf. Typical orbital periods are between 1 and 3 years, but can be significantly larger. There are two principal processes of interaction in such long-period binaries:

(i) Mass loss from the cool component – assumed to be in the form of a wind – represents the primary condition for appearance of the symbiotic phenomenon.

(ii) Accretion of a part of the material lost by the giant by its compact companion. This process generates a very hot ($T_{\rm h} \approx 10^5$ K) and luminous ($L_{\rm h} \approx 10^2 - 10^4\,{\rm L}_\odot$) source of radiation.

On the basis of the way, in which the generated energy is being liberated, we distinguish two phases of symbiotic binary:
A *quiescent phase*, during which the hot component releases its energy approximately at a constant rate and spectral distribution. The hot radiation ionizes a fraction of the neutral giant's wind, but can also be Raman and Rayleigh scattered by its neutral particles. The process of ionization gives rise to nebular emission comprising numerous lines of high excitation/ionization and the continuum. As a result the spectrum of symbiotic stars during quiescence consists of basically three components of radiation – two stellar and one nebular. Figure 1 shows example of such the spectral energy distribution (SED) for AG Peg.
An *active phase*, during which the hot component radiation changes significantly, at least in its spectral distribution. In cases of a nova-like outbursts the luminosity rapidly increases on the timescale of weeks/months, followed by its gradual decrease to the quiescent level within a few years or decades. A common feature of active phases is a high-velocity mass ejection.

The aim of this contribution is to review the recent research results concerning to effects of ionization in symbiotic binaries, which suggest new insight to the nature of some well known phenomena observed in these objects. Section 2 deals with an orbitally-related variation in the light curves during quiescent phases, section 3 summarizes the effect of apparent changes of orbital period during transition from active to quiescent phases, and section 4 discuss some aspects of ionization during active phases.

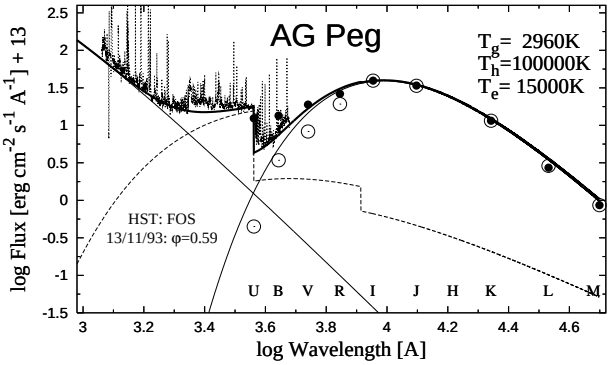

Figure 1: Reconstructed SED in the continuum of AG Peg between 0.12 and 5μm by a three component model of radiation. Solid thin lines are Planck functions, which match the continuum of the cool and the hot star, respectively. Dotted line represents the hydrogen f-b and f-f continuum. The solid thick line is the resulting continuum. Observations were dereddened with $E_{\rm B-V} = 0.1$. More about the fitting procedure is in [49].

2 Ionization during quiescent phases

In this section we discuss the orbitally-related variation observed in the optical/near-UV continuum within a simple ionization model of symbiotic binaries.

2.1 Observations

The most pronounced feature observed in the light curves of symbiotic stars during phases of quiescence is a periodic wave-like variation as a function of the orbital phase. This type of variability was revealed by long-term multicolour photometry made in 1960's [1,2] for AG Peg and Z And. At present, all about 20 symbiotic objects, which have sufficiently covered light curves, display signatures of the wave-like variability during their quiescent phases. It is characterized by a large amplitude $\Delta m \sim 1$ mag or more, which is a function of the wavelength – we always observe $\Delta U > \Delta B \geq \Delta V$. The period is approximately equal to the orbital period, and a minimum occurs at/around the inferior conjunction of the cool component. These properties relate this type of variations to the orbital motion. Figure 2 shows examples of V1329 Cyg, AG Peg, AG Dra, AX Per, BF Cyg and Z And.

2.2 On the nature of the wave-like variation

2.2.1 A reflection effect

Originally, a reflection effect was suggested as responsible for the wave-like modulation in the light curve of AG Peg [3,5]. In this model the hot star irradiates and heats up the facing giant's hemisphere that causes variation in the star's brightness when viewing the binary at different orbital phases. This natural explanation has been adopted by many authors (e.g.: [23,34]), and recently approached quantitatively [39,40]. However, the observed large amplitude makes it difficult to get the model of the reflection effect consistent with observations.

In the model of the reflection effect as approximated by [50], the upper limit (i.e. for $i = 90°$) of the magnitude difference

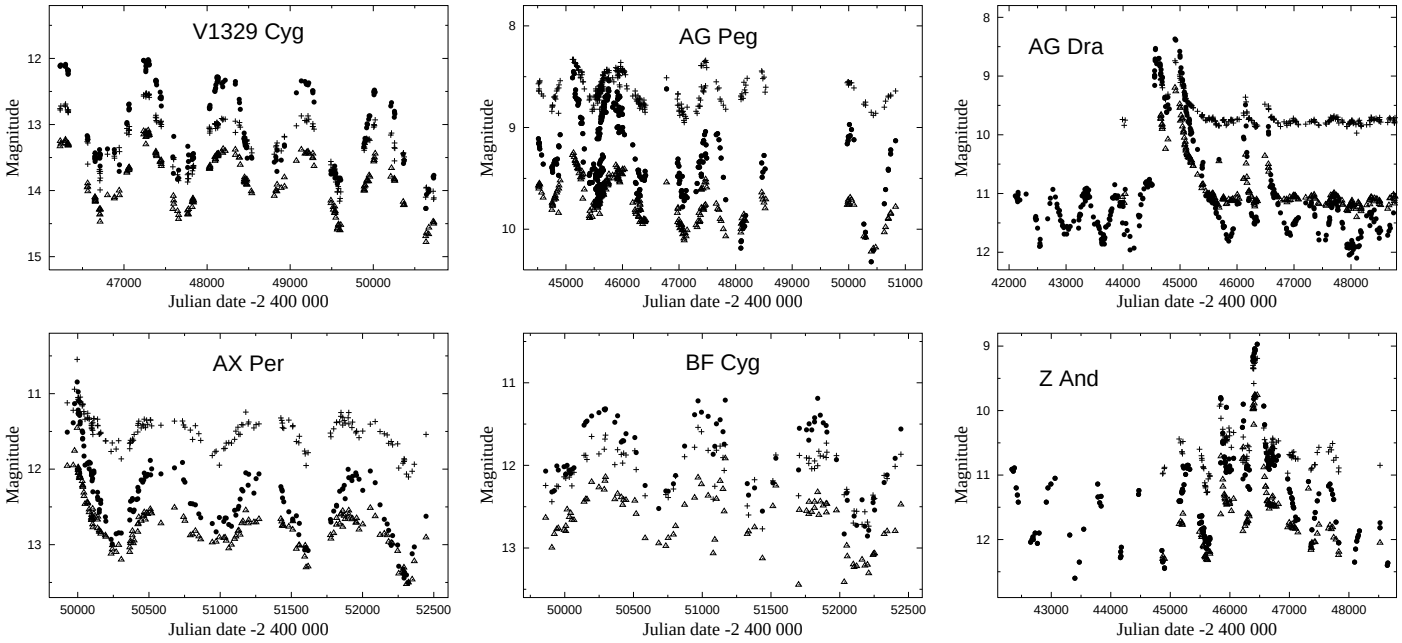

Figure 2: Examples of periodic wave-like variation in the light curves of selected symbiotic binaries. Symbols, •, △ and +, represent observations in the U, B and V band, respectively.

between the two hemispheres, $\Delta m_{\max}$, can be expressed as

$$\Delta m_{\max} = -2.5 \log(1 + 2L_{\rm RE}/L_{\rm g}), \quad (1)$$

where $L_{\rm g}$ is the luminosity of the giant and $L_{\rm RE}$ represents a fraction of the hot star luminosity, $L_{\rm h}$, impacting the giant. For the separation of the stars, $A \gg R_{\rm g}$, $L_{\rm RE} = (R_{\rm g}/2A)^2 \times L_{\rm h}$, and Eq. 1 reads as

$$\Delta m_{\max} = -2.5 \log(1 + \beta/2), \quad (2)$$

where the parameter

$$\beta = \frac{R_{\rm g}^2}{A^2}\frac{L_{\rm h}}{L_{\rm g}} = R_{\rm A}^2 \frac{L_{\rm h}}{L_{\rm g}} \quad (3)$$

measures the strength of the illuminating radiation field relative to that of the giant. So the amplitude of light curves caused by the reflection effect is determined only by the parameter β. However, the parameter β derived from observations can produce a maximum magnitude difference $\Delta m_{\max} < 0.1$ mag, which is far below the observed quantities [50]. On the other hand, the reflection effect (Eq. 2) requires $\beta \geq 1 - 10$ to match the observed amplitudes. Even a more rigorous approach made by [39,40] does not provide a satisfactory explanation of the observed maximum differences in broadband magnitudes for realistic parameters $\beta \approx 0.1 - 0.01$.

Another simplified approach to the reflection effect assumes a clear heating, i.e. the infalled light on the giant's hemisphere is absorbed and transformed into the heating up it. In this case the temperature of the irradiated hemisphere increases in maximum by a few $\times$ 10 K for typical quantities of a symbiotic binary (see Eq. B.9 of [39]. Such small temperature difference between the two hemispheres cannot cause the observed amplitude in the light curves (e.g.: [3]). In a more realistic case, in which the giant's wind is ionized by the hot component radiation, only photons not capable of ionizing hydrogen ($\lambda > 912$ Å) can penetrate into the HI zone at a vicinity of the giant's photosphere (Sect. 2.2.2, Fig. 3). In addition, a part of them (mainly those from the hot stellar source at the far-UV) are Rayleigh scattered by the neutral part of the red giant wind (particle density $n \sim 10^{10}{\rm cm}^{-3}$). As a result the real heating effect will probably be negligible. This is in agreement with observations of [44], who did not find any irradiation effect in the red giant spectrum of SY Mus, although its visual light curve varies with an amplitude of 0.6 mag.

Finally, occultation of a bright gaseous region by the stellar disk of the giant in the system was recently considered to explain the light variation in the U band of AG Dra [59]. The nature of this emission region is seen in photoionization of the giant's wind. The authors assumed that this region is located most probably around the hemisphere of the giant facing the hot component. In the cases of a sinusoidal shape of the orbitally-related light variation (e.g. V1329 Cyg, AG Peg, AG Dra, Z And; Fig. 2), about 50% of the light, which is subject to variation, should still be occulted at the orbital phases 0.25 and 0.75, when viewing the binary from its side. However, the extra emission region is physically displaced from the giant's photosphere (the HI/HII boundary lies at 0.33 A from the giant in AG Dra on the line connecting the stars [50]), therefore a simple geometrical occultation cannot be responsible for such large loss of the light at these phases, mainly for the objects with $i \ll 90^\circ$.

2.2.2 An ionization model and the wave-like variability

All these reflection(-like) effects mentioned above assume the extra emission region to be localized at/on the giant's photosphere. This implies two main problems in explanation of the observed large magnitude variations: (i) A low emission of geometrically small region, and (ii) its localization under condi-

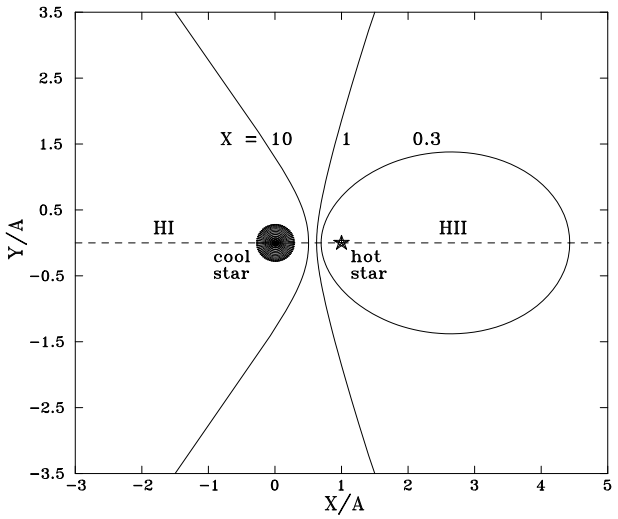

Figure 3: The HI/HII boundary calculated for X = 0.3, 1, 10, the stellar wind model characterized by the parameters γ = 2.5 and $R_{\rm g}/A$ = 0.28 (see [50] for more detail).

tions of symbiotic binaries. Therefore we outline the nature of the orbitally-related changes in the optical/near-UV continuum within an ionization model of symbiotic binaries, i.e. within the basic model of symbiotic stars as introduced in section 1.

A zero-level ionization model. The extent of the ionized zone can be obtained from a parametric equation

$$f(r,\vartheta) - X = 0, \tag{4}$$

the solution of which defines the boundary between neutral and ionized gas at the orbital plane determined by a system of polar coordinates, r, ϑ, with the origin at the hot star [45]. By other words the ionization boundary is defined by the locus of points at which ionizing photons are completely consumed along paths outward from the ionizing star. The function $f(r,\vartheta)$ was treated for the first time by [45] for a steady state situation (a constant velocity of the wind and no binary rotation) and pure hydrogen gas. The parameter X is given mainly by the binary properties – separation of the components, number of hydrogen ionizing photons, terminal velocity of the wind and the mass-loss rate (for details see [36,45]). The particle density of the ionized material is given by the velocity distribution of the giant's wind, which is here assumed to be of the form

$$v_{\rm wind} = v_\infty (1 - R/r)^\gamma, \tag{5}$$

where r is the distance from the center of the cool star, R is the origin of the stellar wind ($\approx$the radius of the giant) and v_∞ is the terminal velocity of the wind. The parameter γ characterizes an acceleration of the wind. A larger γ corresponds to a slower transition to v_∞. Figure 3 shows examples of the HI/HII boundary for X = 0.3, 1, 10 and the parameter γ = 2.5 in the wind model.

Amount of emission from the model and observations. Here we show that the nebular emission in the continuum produced by this model can balance that given by observations. The nebular flux largely depends on the number of hydrogen recombinations, and is proportional to $\int n_+ n_{\rm e}\, dV$, (the so called emission measure - EM); n_+ and $n_{\rm e}$ is the concentration of ions (protons) and electrons, respectively.

Table 1: Observed and calculated EM for selected objects.

Object	$F_\lambda^{\rm obs}/10^{-13}$	$EM_{\rm obs}$ [cm^{-3}]	$EM_{\rm M}$ [cm^{-3}]
BF Cyg	5.0^a	3.8×10^{60}	2.9×10^{60}
BF Cyg	2.7 - 7.9^b	3.6 - 10×10^{60}	
AG Dra	2.4 ^{a}	1.5 ×10^{59}	1.5×10^{59}
AG Dra	0.9 - 2.2^b	0.5 - 1.3×10^{59}	
AX Per	2.0^a	2.1×10^{59}	1.2×10^{59}
AX Per	1.0 - 2.5^b	1.8 - 4.6×10^{59}	
V443 Her	2.1^a	3.0×10^{59}	4.2×10^{59}
V443 Her	1.1 - 2.1^b	2.7 - 5.2×10^{59}	

a - from the energy distribution in the spectrum at λ3646$^-$Å.
b - from the dereddened U-magnitude at minimum and maximum, respectively.
Flux in units of erg cm^{-2} s^{-1} Å^{-1}

(i) *Observations:* The quantity of the EM can be estimated, for example, from the measured flux, $F_\lambda^{\rm obs}$ (erg cm^{-2} s^{-1} Å^{-1}), of the nebular continuum at the wavelength λ, as

$$EM_{\rm obs} = 4\pi d^2 F_\lambda^{\rm obs}/\varepsilon_\lambda, \tag{6}$$

in which d is the distance to the object, ε_λ is the volume emission coefficient. The nebular flux can be obtained from the energy distribution in the spectrum. Its upper limit can also be estimated from the dereddened U-magnitude if the nebular continuum dominates the optical.

(ii) *Model:* The source of the nebular radiation in the model is the ionized region, in which the rate of ionization/recombination processes is balanced by the rate of photons, $L_{\rm ph}$ (photons s^{-1}), capable of ionizing the element under consideration. In the case of pure hydrogen we can write the equilibrium condition as $L_{\rm ph} = \alpha_{\rm B} \int_V n_+(r) n_{\rm e}(r)\, dV$, where $\alpha_{\rm B}$ (cm^3 s^{-1}) is the total hydrogenic recombination coefficient and $L_{\rm ph}$ is given by the luminosity and temperature of the hot star. So the quantity of the emission measure given by the model ($EM_{\rm mod}$) can be written as

$$EM_{\rm mod} = L_{\rm ph}/\alpha_{\rm B}. \tag{7}$$

Having independently determined $L_{\rm ph}$ we compare the EM given by observations (Eq. 6) and that required by the ionization model (Eq. 7). Results for some objects are in Table 1, which demonstrates that

$$EM_{\rm obs} \sim EM_{\rm mod}. \tag{8}$$

So the amount of emission produced by the ionization model is consistent with observations.

Variation in the EM and light curves. Here we show that the variation in the EM is responsible for the investigated wave-like variation in the light curves.

The quantity of the EM also varies as a function of the orbital phase (e.g.: [11,31]). In Fig. 4 we show an example of the SED of AG Dra at the orbital phase 0.46 and 0.91, i.e. close to its maximum and minimum, respectively. This demonstrates that the nebular continuum emission is subject to variation with

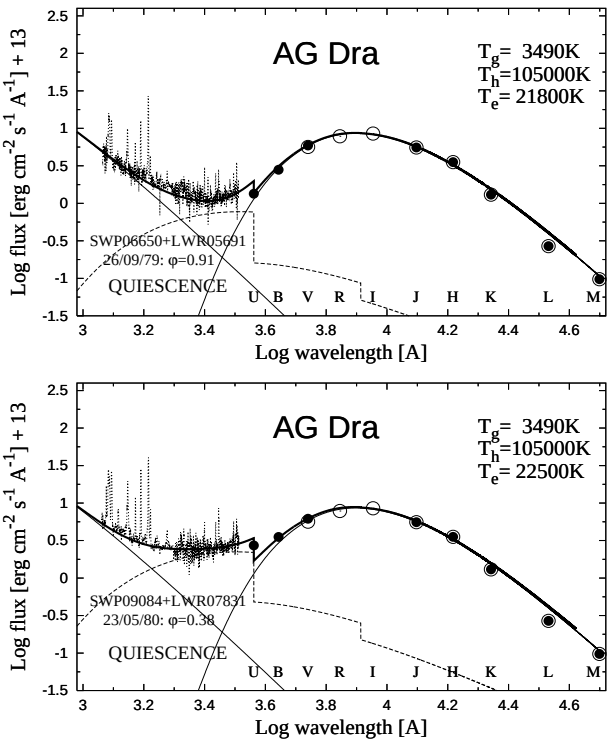

Figure 4: Example of the SED of AG Dra at the orbital phase 0.91 (top) and 0.46 (bottom), which demonstrates the orbital variability in the nebular emission.

the orbit of the binary. To compare the observed variability in EM to that in the light curves, we express Eq. 6 in the scale of magnitudes ($m_\lambda = -2.5\log(F_\lambda) + q_\lambda$) as

$$m_\lambda = -2.5\log(EM) + C_\lambda, \tag{9}$$

where

$$C_\lambda = q_\lambda - 2.5\log\left(\frac{\varepsilon_\lambda}{4\pi d^2}\right), \tag{10}$$

in which the constant q_λ defines magnitude zero. Using Eq. 9 we constructed the light curves from the measured values of the EM in BF Cyg and Z And and compared them to those obtained photometrically. We adopted distances d = 4.6 and 1.12 kpc for BF Cyg and Z And, respectively. Figure 5 shows that the variation in the EM follows well that observed in the light curves (see [50] for details). Finally, we need to answer the question: "What is the origin of the periodic wave-like variability?" So,

Why does the emission measure vary? To explain the orbitally-related variation, the nebula has to be partially optically thick and of a non-symmetric shape (Sect. 3.2.1) to produce different contributions of its total emission into the line of sight at different orbital phases. In our simple ionization model the opacity, κ, of the ionized emission medium decreases with the distance from the cool star, since $\kappa \propto n \propto r^{-2}$ (i.e. the parts nearest to the giant's photosphere will be most opaque). From this point of view, shaping of the optically thick portion of the HII zone will be given by the parameter X in our ionization model (Eq. 4, Fig. 3). To characterize the basic shape of the *observed* light curves [47] introduced a parameter a as

$$a = \frac{m(0) - m(0.25)}{\Delta m_{\max}}, \tag{11}$$

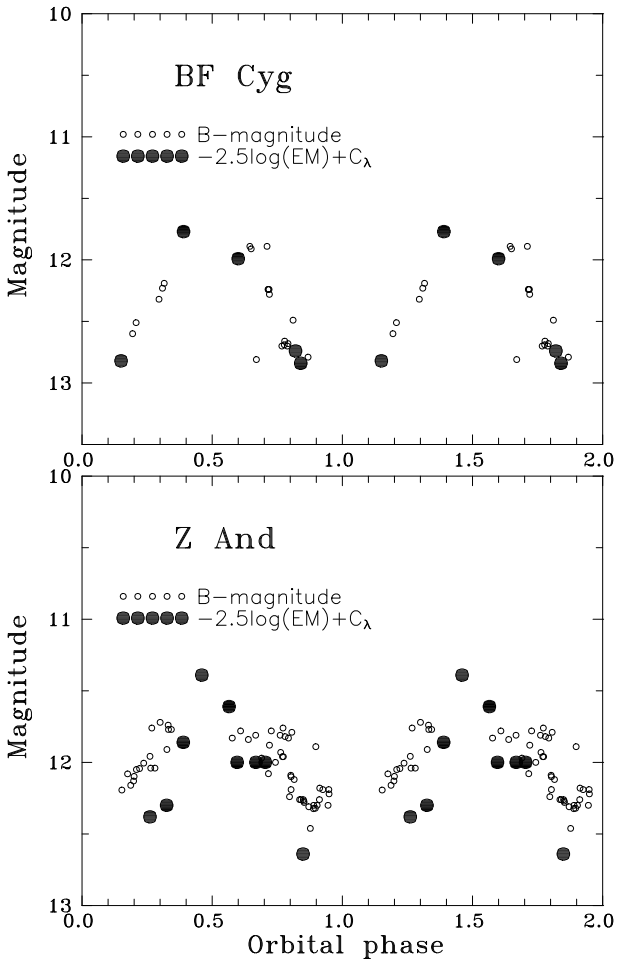

Figure 5: Top: Variation in the EM of BF Cyg as a function of the orbital phase. The data [31] were converted into the B-magnitudes according to Eq. 9. Compared is the light curve in the B band obtained photometrically during the same period [21]. Bottom: The same as the top, but for Z And. Measurements of the EM were taken from [11], and photometric B-magnitudes from Fig. 1, but omitting the active phase. These results show that the variation in the EM is fully responsible for that in the light curves (from [50]).

where $m(0)$ and $m(0.25)$ are the magnitudes at the orbital phases 0 and 0.25, respectively, and $\Delta m_{\max}$ is the amplitude of the light curve. The shape of the light curve resembles a sinusoid for $a = 0.5$, but $a > 0.5$ implies a broader maximum than minimum. [50] found a relationship between the parameter a and the parameter X (Fig. 6). This supports a connection between the shape of light curves and the extent of symbiotic nebulae. Accordingly, [50] suggested a qualitative description on how the observed profile of light curves could be produced within the ionization model mentioned above:

(i) In the extensive emission zone ($X \geq 10$), the partially optically thick portion of the HII region has the geometry of a cap on the HI/HII boundary around the binary axis. This mimics the reflection effect, but the emission region causing the light variation is physically displaced from the giant's surface. In this case the light curve profile is a sinusoid characterized by the parameter $a \leq 0.5$ (e.g. V1329 Cyg, Z And, AG Dra).

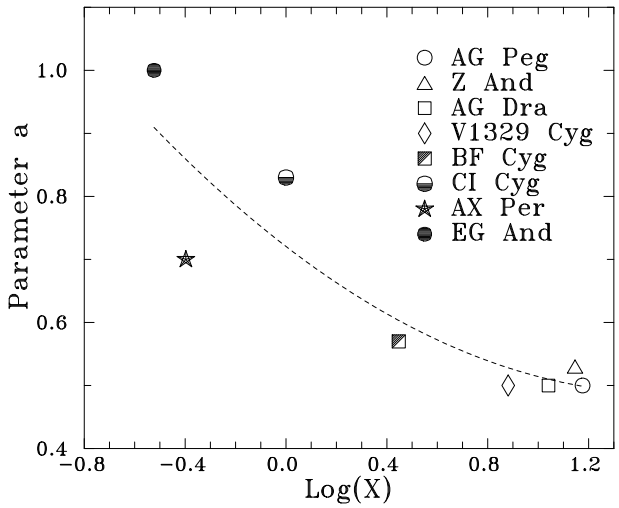

Figure 6: A correlation between the shape of the light curve characterized by the parameter a (see the text) and the extent of the symbiotic nebula given by the parameter X (from [50]).

(ii) In the case of an oval shape of the HII zone (Fig. 3, a small parameter X), its total emission will be attenuated more at positions of the inferior and superior conjunction of the cool star (the orbital phase φ = 0 and 0.5, respectively) than at positions of φ = 0.25 and 0.75, respectively. Such apparent variation in the EM can produce a primary as well as secondary minimum in the light curve. This type of the light curve profile corresponds to the parameter $a \sim 1$ (e.g. EG And). A gradual opening of the HII zone (approximately $0.3 < X < 1$) will make it optically thinner behind the hot star (outside the binary around φ = 0.5). Therefore the secondary minimum will become less pronounced or flat, and/or a maximum at $\varphi \sim 0.5$ can arise. The light curve profile here should be characterized by the parameter $a > 0.5$ (e.g. CI Cyg, AX Per). However a quantitative approach to determine opacities of a more realistic structure of the ionized region in symbiotic binaries is required.

3 Ionization during transition periods

In this section we discuss the role of ionization in symbiotic binaries during their transition from active to quiescent phases. Based on analysis of the long-term photometric observations of a group of classical symbiotic stars, it was shown that a transition between different levels of activity produces a systematic variation in the $O-C$ residuals and thus an apparent change in the orbital period [48].

3.1 Systematic variation in the O-C residuals

Here we demonstrate this effect on historical light curves of classical symbiotic stars BF Cyg and AG Peg. First, we determine positions of the observed minima in their light curves. Second, we construct the $O-C$ diagram using a reference (spectroscopic) ephemeris. By this way we get a relative position between the time of the inferior conjunction of the cool star and the observed light minimum, i.e. the location of the main emission source in the binary with respect to the line connecting the stars.

BF Cyg ($P_{\rm orb}$=757.3 days): Top left panel of Figure 7 shows the historical light curve with the $O-C$ diagram of BF Cyg. As the reference ephemeris we adopted that given by all the primary minima measured by [48],

$$JD_{\rm Min} = 2\,411\,268.6 + 757.3(\pm 0.6) \times E, \qquad (12)$$

which is identical (within uncertainties) with the spectroscopic ephemeris of [10]. A systematic variation in the $O-C$ residuals is clearly seen. This behaviour was already noted by [22]. An increase before the 1920 bright stage (E = 1 to 11) corresponds to a period of 770 days, while the subsequent decrease (E = 12 to 24) indicates a shorter period of 747.5 days. The same type of variability appeared again during the recent, 1989 active phase. Observed changes in both the position and the shape of the minima are illustrated in the top right panel of Fig. 7. During the transition *from the active phase to quiescence* (the $A \rightarrow Q$ transition), a systematic change in the minima positions at E = 49 to 51 corresponds to a period of 730 days. The following minima (E = 52, 53 54), which were observed during quiescent phase, do not exhibit any systematic change in their position. During the transition *from the quiescent to the active phase* ($Q \rightarrow A$), a significant change in the $O-C$ values by jump of +130 days was observed. The minima at E = 45 to E = 49 indicate an apparent period of 794 days.

AG Peg ($P_{\rm orb}$=812.6 days): As the reference ephemeris for timing of the inferior conjunction of the cool giant in AG Peg we can adopt that of [48]

$$JD_{\rm sp.conj.} = 2\,427\,664.2(\pm 10) + 812.6(\pm 1.8) \times E, \qquad (13)$$

which is based on about 20 orbital cycles during 1945 – 1992.

From ∼1940 the light curve developed a periodic wave-like variation [28]. The periodic variability has been very intensively studied. The real shifts of the observed minima from the predicted positions were often noted [4,26,27]. As a result, many different periods ranging from ∼730 to ∼830 days were suggested ([25] and references therein). Generally, the older data gave a longer period (e.g.: [28]) than the more recent observations (e.g.: [12]). Figure 8 shows the photographic and visual light curves from 1935. Characteristic points (mostly maxima and minima) were taken from photographic measurements [28], while the visual data represent smoothed AFOEV (Association Francaise des Observateurs d'Etoiles Variables) estimates available from CDS. Positions of the observed minima define the ephemeris

$$JD_{\rm Min} = 2\,427\,495.9 + 820.3(\pm 0.8) \times E. \qquad (14)$$

To confirm the real difference between both the photometric and the spectroscopic period, we divided the available data set of radial velocities into two parts: (i) The old data from 1945.8 to 1973.8 (24 measurements), and (ii) the more recent data from 1978.5 to 1992.0 (58 measurements). Then we solved circular orbits for each data set separately with fixed period of 820.3 days. Both solutions differ from each other only in the time of spectroscopic conjunction corresponding to an average shift of 0.15 $P_{\rm orb}$ between them (Fig. 9 top). However, the phase diagram of all radial velocities constructed for the elements in Eq. 13 does not display any systematic shift (Fig. 9 bottom). This means that the

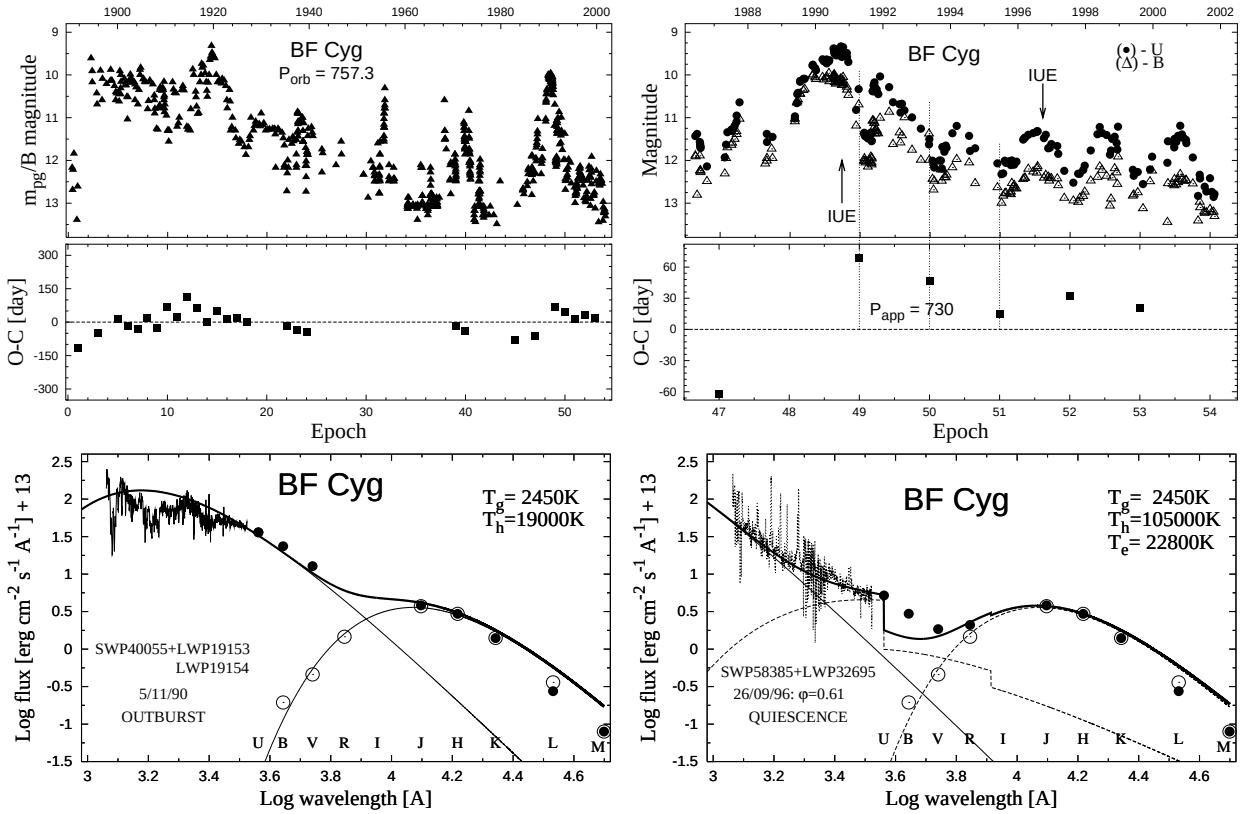

Figure 7: Top: Historical and recent light curves of BF Cyg with the $O-C$ diagrams for the observed minima. During the recent transition to quiescence (E = 49, 50, 51), an apparent period of 730 days was indicated. Bottom: The SED during the active and the quiescent phase. This together with the change in the shape and position of the minima demonstrate the change in the geometry and location of the symbiotic nebula during the $A \rightarrow Q$ transition.

photometric period is inconsistent with the *orbital* period, and thus represents an apparent period in the system. The $O-C$ residuals display a systematic increase along a gradual decrease of the star's brightness. Such behaviour reflects a longer apparent period than the orbital one.

3.1.1 Common properties

By this way [48] analyzed other 5 symbiotic systems (CI Cyg, V1329 Cyg, Z And, AG Dra and YY Her) and found following two main characteristics in the variation of the $O-C$ residuals:

1. *Systematic variation in positions of the minima is connected with a variation in the energy distribution of the hot component radiation.*

The effect is very striking when also the nature of the hot continuum changes – from a blackbody during outburst to a nebular radiation in a quiescence. In this case the apparent period is shorter than the orbital one. Figure 7 demonstrates this case for the eclipsing system BF Cyg on its SED during the 1990 outburst and the following quiescent phase.

The case, in which no change in the nature of the hot continuum was observed, we demonstrated on the example of AG Peg (Fig. 8). At the beginning of its nebular phase, when the wave-like variation developed in the light curve (from $\sim$1940), the minima were shifted by about -100 to -200 days from their prediction by Eq. 13. Then, the following minima were appearing systematically closer to the time of conjunction. In such the case the apparent period is larger than the orbital one. Also here behaviour in the $O-C$ residuals was followed by a gradual decline of the star's brightness.

2. *Separation between the minima correlates with the velocity of the brightness variation.*

Generally, a fast and large change in the period is indicated during $Q \rightarrow A$ transitions, when the brightness changes rapidly. Contrary, $A \rightarrow Q$ transitions, during which the star's brightness declines slowly, produce a smaller change in the period. [48] determined a relation between parameters $\Delta m/\Delta t$ and $\Delta P/P_{\rm orb}$ characterizing the velocity of the change in the star's brightness and the corresponding phase shift in the period, respectively, for different transition epochs in a larger sample of symbiotic stars as

$$\frac{\Delta P}{P_{\rm orb}} \sim 134 \frac{\Delta m}{\Delta t}, \qquad (15)$$

where the parameter $\Delta m/\Delta t$ is in mag/day.

3.2 Principle of apparent orbital changes

Generally, the shape and position of a minimum in the light curve reflect the geometry and location of the main source of the optical continuum in the binary. In symbiotic binaries the nebular radiation often dominates the optical continuum during quiescence (cf. Fig. 1), but significantly changes during active phases (Fig. 7). Therefore the observed photometric variations are caused mainly by changes of the ionization structure in symbiotic binary

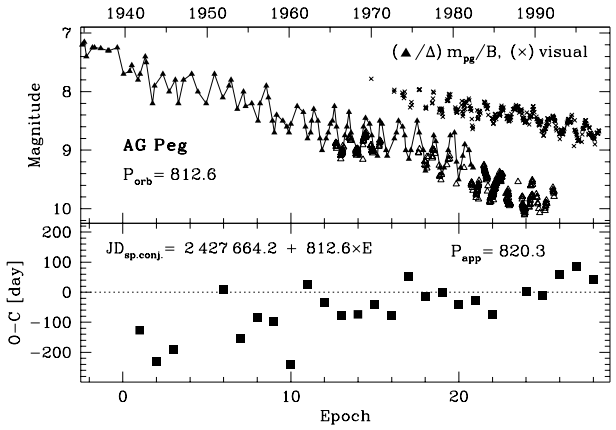

Figure 8: Top: Compiled photographic/B and visual light curves of AG Peg as recorded from 1935. Bottom: The $O-C$ diagram for the observed minima. A gradual increase in the $O-C$ values indicates an apparent period of 820.3 days.

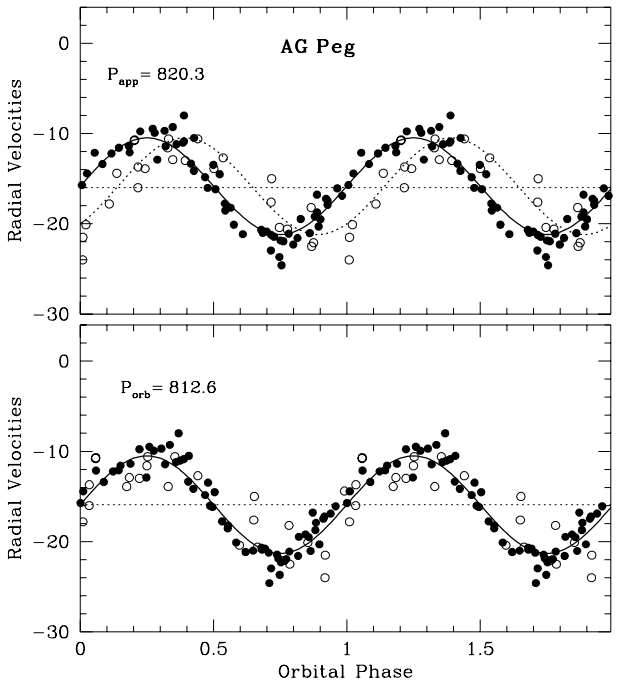

Figure 9: Top: The old, 1945.8 - 1973.8, radial velocities (open circles) and the more recent, 1978.8 - 1992.0, measurements (full circles) are shifted by $\sim$0.15 $P_{\rm orb}$ relative to each other when folded with the photometric period of 820.3 days. Bottom: No systematic shift can be seen when the data are folded with the orbital period of 812.6 days.

due to outbursts, i.e. due to variation in the luminosity of ionizing photons. Basically, there can be recognized two different sources of the hot continuum in the symbiotic system – a relatively cool and small pseudophotosphere around the hot component and the extended asymmetrical HII zone – dominating the optical spectrum during active and quiescent phases, respectively (Fig. 7). Thus, during outbursts we can observe deep narrow minima – eclipses – at the position of the spectroscopic conjunction, while during quiescence the minima are broad, complex in profile, and shifted from the position of the spectroscopic conjunction (here BF Cyg). A systematic change in timing of the minima can occur also if only the luminosity of ionizing photons changes, without any creation of a cool pseudophotosphere around the hot star, because this also produces a systematic variation in the shape of the HII zone (here AG Peg). However, the variation is not so drastic as can be observed in the former case.

3.2.1 Asymmetric shape of the H II zone

Observation of the systematic variations in the $O-C$ residuals suggests an asymmetrical shape of the HII zone with respect to the binary axis to describe the observed apparent changes in the orbital period. There are also some observational arguments and calculations suggesting the asymmetrical shape of the HII zone:

(i) Direct observational evidence of an asymmetrical HI (and thus also HII) region is represented by a wide 'eclipse', lasting from the orbital phase $\sim$0.9 to $\sim$1.6, in the far-UV region caused by Rayleigh scattering in BF Cyg [38].

(ii) Asymmetric shape of the ionization front is suggested by spectropolarimetric studies of [41,42]. The geometry of the HII zone has no symmetry with respect to the binary axis to explain the observed polarization properties. In these models, due to the orbital motion, the ionization front in the orbital plane is twisted, going from the side of the hot star that precedes its orbital motion, through the line joining the components, to the front of the cool star against its motion.

(iii) Asymmetrical nebular geometry is also suggested by hydrodynamical calculations of the structure of stellar winds in symbiotic stars that include effects of the orbital motion. The recent models [14,66,67] are characterized by the S-shaped wind-collision zone, placed in the binary likewise as the ionization front described in the point (ii).

(iv) Finally, [50] introduced a modification of the simplest steady state ionization model as introduced in Sect. 2.2.2 by including the orbital motion and a velocity structure of the giant's wind. In this model the HII zone for small values of the X parameter is also asymmetrically placed in the binary with respect to the binary axis. Figure 10 shows this case.

Therefore we can assume that the shape of the optically thick fraction of the HII region is prolonged in a direction between the stars and its projection into the orbital plane is inclined relatively to the binary axis, probably shaped as described in the point (ii).

3.2.2 The cases of BF Cyg and AG Peg

A *gradual* decrease in the star's brightness results in a *systematic* variation of the structure of the HII region, which then produces the observed variation in the $O-C$ residuals and thus an apparent change in the period. Here we distinguish two situations:

(i) A *decrease* of the total luminosity, as during nebular stage of AG Peg (the nature of the optical continuum is not changed), produces also a decrease of the luminosity of the hydrogen ionizing photons. This leads to a gradual shrinking of the HII zone, and thus the minimum can be expected to occur prior, but closer to the position of the spectroscopic conjunction than during the previous cycle. As a result a larger apparent period than the orbital one is observed.

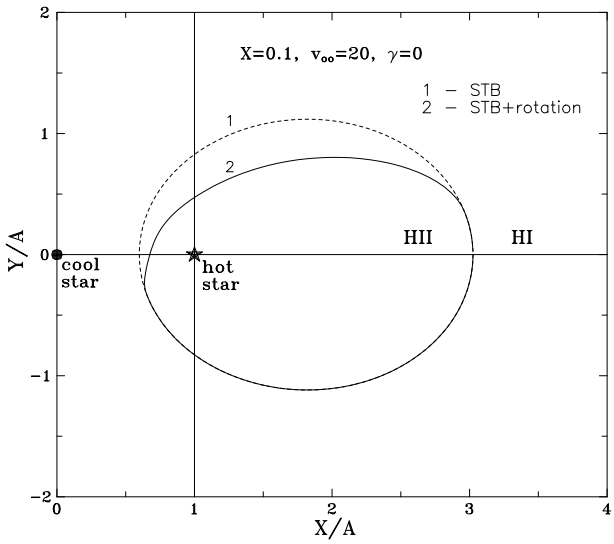

Figure 10: The HI/HII boundary given by the steady state ionization model (dashed line) and its modification due to the orbital motion (solid line). This model was calculated for $P_{\rm orb}$ = 757 days, separation between the binary components A = 465 $\mathrm{R}_\odot$ and the mass ratio $q = 6$. The binary rotates anti-clockwise ([50]).

(ii) An approximately *constant* hot star bolometric luminosity during a gradual decrease of the star's brightness throughout the $A \rightarrow Q$ transitions of BF Cyg, produces an increase in the luminosity of the ionizing photons as the temperature of the hot star increases. This is connected with a significant change in the nature of the optical continuum – from a blackbody to a nebular radiation (Fig. 7), which causes an expansion of the HII zone that fits gradually its prolonged shape. The light minima, contrary to the case (i), will occur prior to, but systematically further from the time of spectroscopic conjunction. As a result, a shorter apparent period than the orbital one is indicated, and the minima become broader. Contrary, during $Q \rightarrow A$ transitions in these objects a rapid decrease in the luminosity of the $L_{\rm ph}$ photons results in practical disappearance of the HII region, and a cool pseudophotosphere around the hot star is created. Therefore the minima – eclipses – are observed at the spectroscopic conjunction and a sudden apparent change in the period by jump is indicated (Fig. 7, minima just before the 1989 outburst).

4 Ionization during active phases

Outbursts of symbiotic stars were originally recognized on the basis of their photometric evolution. The most pronounced common feature of all active classical symbiotic stars (*ClSS*) is an increase in the star's brightness, typically by 2-3 mag, on the timescale of weeks and with the amplitude increasing toward shorter wavelengths. The maximum is followed by a gradual decrease to quiescence conditions within several months or years. However, the light curve profiles and the recurrence of the outbursts are very different from object to object. In some cases active phases are characterized by multiple maxima (AG Dra, Z And), in cases of AX Per and AR Pav the optical light during activity waves as a function of the orbital phase and the case of CH Cyg has no counterpart among other symbiotics – its active phases produce variations in the optical continuum up to 6 mag with superposed changes on the time-scale of weeks/hours to seconds. Finally, BF Cyg displays three different types of outbursts (a symbiotic nova eruption, that observed in *ClSS* and flares) in its historical light curve [53].

Further common observational property of the *ClSS* outbursts is a mass-outflow from the active star in the form of an optically thick expanding shell or a fast stellar wind detected spectroscopically by profiles of the P-Cygni type and/or by broadening of emission lines. In the radio and for the nearest objects (e.g. CH Cyg, R Aqr) the bipolar shaped ejecta (jets) were detected. Information about the mass-outflow are, however, sensitive to timing of spectroscopic observations (e.g. signatures of the mass ejection are better seen at the beginning of outbursts) and the ionization structure of the symbiotic nebula (profiles of the highly ionized elements can still be rather narrow as they originate at the vicinity of the ionizing source, where the material is accelerated to a low velocity). In addition, the resulting picture depends on the inclination angle.

To recognize the nature of the contributing lights during outbursts we use here a method of analyzing their SED in the 0.12-5.0 μ and distinguishing between eclipsing and non-eclipsing systems. This allow us to quantify individual components of radiation and to point basic properties of the mass ejection during active phases of *ClSS*. As an example, we introduce a simple Hα method to estimate the mass-loss rate during active phases of CH Cyg.

4.1 Eclipsing system CI Cyg

CI Cyg is well known eclipsing system with an orbital period of 855 days. A detailed study of CI Cyg made by [24] suggests that this system contains an M5 II giant ($M_{\rm g} \sim 1.5\,\mathrm{M}_\odot$) and a hot ionizing source ($M_{\rm h} \sim 0.5\,\mathrm{M}_\odot$, $T_{\rm h} \sim 10^5$ K), with a high inclination of the orbit. Fig. 11 shows evolution of the light curve from its major eruption in 1975. It provides striking constraints on the structure and nature of the source of the optical light. The narrow minima during the first four cycles from the maximum suggest the source of the optical continuum to be formed in a small volume (in the binary dimensions) centered on the hot star. This implies that the nebular contribution was negligible at the maximum. Contrary to this behaviour, during subsequent cycles, the broad minima in the continuum developed. The near-UV/optical spectrum was dominated by the nebular emission and the lines of highly ionized elements [24].

Our fit of the CI Cyg SED confirms these results (Fig. 11). In addition, such approach allow us to quantify individual components of radiation and to determine the corresponding parameters. During the active phase a warm blackbody component of radiation ($T_{\rm h}$ = 20 500 K) with superposed highly ionized lines dominated the ultraviolet (bottom left panel of Fig. 11). The fit suggests the presence of rather faint nebular emission of a very low electron temperature ($T_{\rm e}$ = 7 600 K). Both components are subject to eclipse and thus occupy a small region around the central star. During transition to a quiescent phase (from about 1984) the SED in the UV converted to that typical for quiescent phases (bottom right panel of Fig. 11, Fig. 1). This reflects a strong change in the ionization structure, which is also connected with indication of an apparent change of the orbital period as dis-

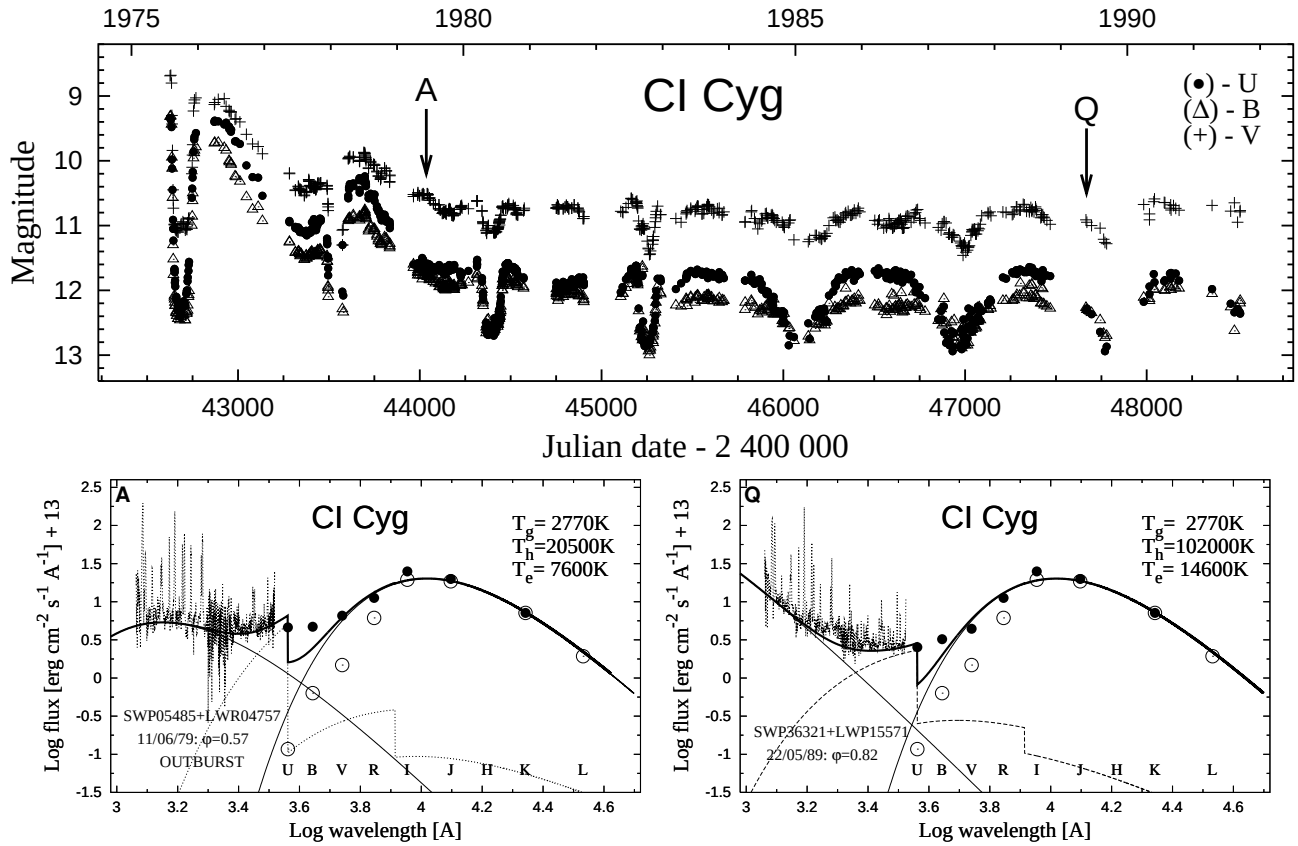

Figure 11: Top: The light curve of CI Cyg covering the period from its outbursts in 1975 to 1993. From about 1984 the system converted to a quiescent phase, which is characterized by the wave-like orbitally-related variation. The data were summarized from the literature. Bottom: The SED during the active phase (left) and quiescence (right). This demonstrates a strong change in the ionization structure of the CI Cyg nebula between both phases (see the text).

cussed in Sect. 3 (see [48] for more details). The hot star has a temperature $T_{\rm h}$ ∼100 000 K and the nebula occupies a large volume in the binary.

4.2 Non-eclipsing system AG Dra

The binary of AG Dra has an orbital period of 550 days (e.g.: [15]) and consists of a K-type giant [35] with a mass of $M_{\rm g} \sim 1.5\,{\rm M}_{\odot}$ and probably a hot white dwarf of $M_{\rm h} \sim 0.5\,{\rm M}_{\odot}$ and $T_{\rm h} \sim 0.9 - 1.3 \times 10^5$ K embedded in a dense nebula [17,32,43]. There are no signs neither in the optical nor far-UV regions of eclipses. Based on spectropolarimetric observations [43] derived the orbital inclination $i = 105 - 140°$.

The system undergoes occasional eruptions, during which the star's brightness abruptly increases ($\Delta U \sim 2$, ΔV ∼1 mag) showing multiple maxima separated approximately by 1 year (Fig. 12). During eruptions the hot component develops a fast wind at a few $\times 10^2 - 1\,300\,{\rm km\,s^{-1}}$ [60,61,62]. The spectral energy distribution of the continuum shows a strong nebular component dominating the UV/U-band region mainly during the activity (Fig. 5 of [18], Fig. 12 here). The quiescent phase of AG Dra is characterized by a periodic wave-like variation in the optical continuum, which is more pronounced at short wavelengths ([46], Fig. 12).

A precise fitting of the SED of the AG Dra continuum (Fig. 4 and bottom panels of Fig. 12, see [49] for more details) clarifies following points:

(i) Nature of a very different amplitude of the wave-like variation in the UBV bands. As only the nebular emission is the subject to the wave-like variability (Sect. 2.2.2, Fig. 4), and its contribution in the optical is very small with respect to that from the giant photosphere, the amplitude in B and V is therefore very small with respect to that in U.

(ii) Nature of the UV/optical continuum during active phases. The SEDs show that the nebular component of radiation is present during both the quiescent and the active phases. In quiescence it dominates the near-UV with electron temperature $T_{\rm e} \approx 20\,000$ K, but in outbursts it represents the strongest component between about 1 500 Å and the V band with $T_{\rm e} \approx 30\,000$ K. Also the stellar component of the hot star radiation increased considerably by a factor of about 10 during the 1981-82 active phase. This point is important for comparison to the eclipsing systems.

4.3 A mechanism of outbursts

A strong nebular component of radiation develops immediately at the beginning of each outburst of AG Dra (Fig. 12, [57]). This is in strong contrast to eclipsing systems of BF Cyg (Fig. 7) and CI Cyg (Fig. 11), in which the hot stellar component is replaced by a warm, ∼20 000 K, blackbody radiation at the beginning of their outbursts. On the other hand, a high-velocity mass-outflow represents a common property of outbursts in all systems.

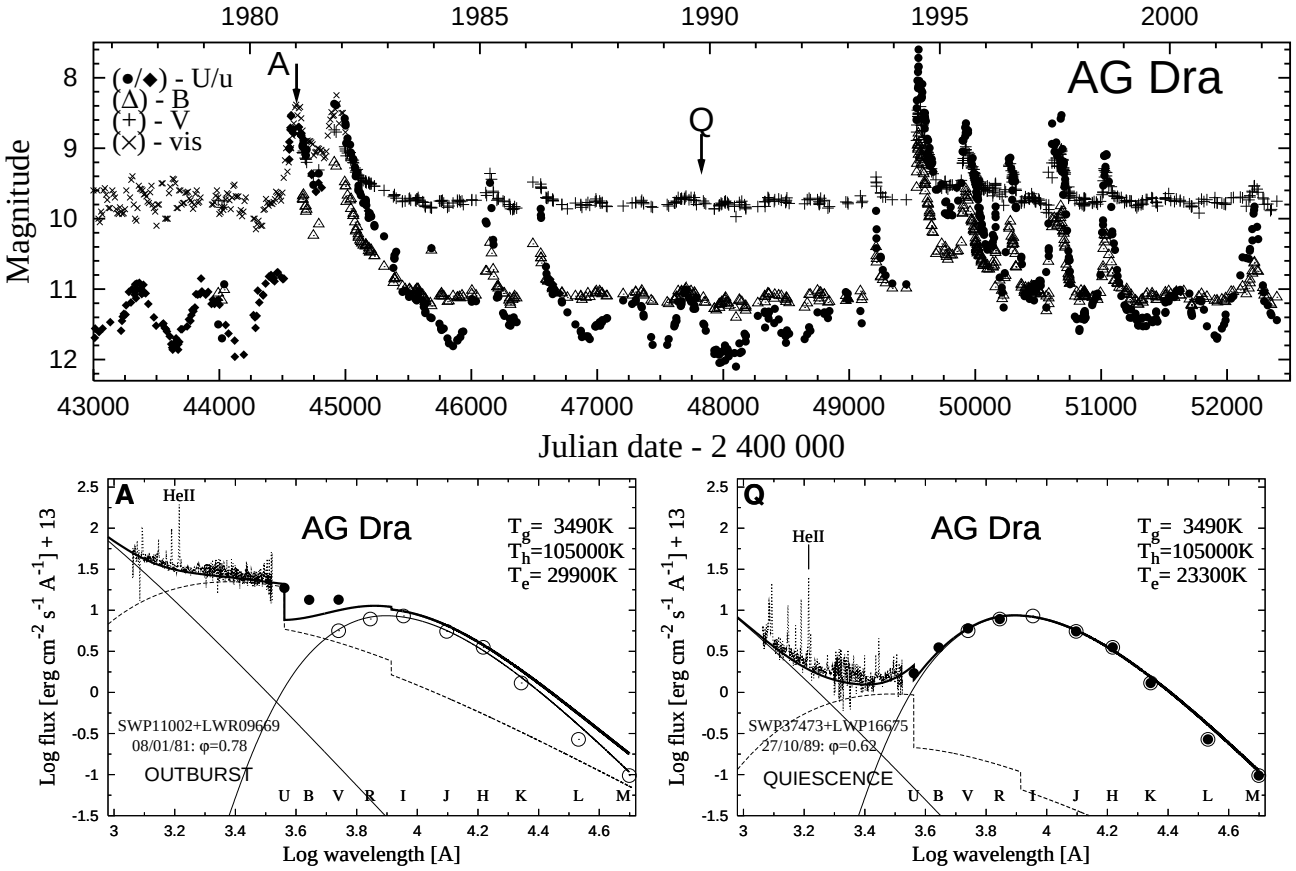

Figure 12: Top: The light curve of AG Dra covering the period from 1976.7 to 2002.5. Quiescent phases (to 1981 and 1987-1994.5) are characterized by the orbitally-related variation, while the active phases by multiple eruptions (1981-82, 1985-86 and 1994-99). In both cases the variability is most pronounced in the U band. The data were summarized from the literature. Bottom: The SED during the 1981 active phase (left) and quiescence (right) of the symbiotic binary AG Dra. This shows a significant contribution of the nebular component of radiation during both phases of AG Dra.

These properties (a mass outflow, but the very different nature of the UV continuum) can be interpreted as an inclination effect if the outburst's mechanism of the mass ejection is of the same nature in both types of systems.

Eclipsing systems: The simultaneous presence of a cool pseudophotosphere with the superposed highly ionized lines in the ultraviolet suggests an optically thick disk-like torus encompassing the hot star to be coincident with the orbital plane. Such the formation in the system obscures a fraction of the hot star radiation and redistributes it into longer wavelengths. The rest part of the hot star flux ionizes the regions above/below the disk and thus gives rise to highly ionized lines. The disk is subject to eclipses, so its dimension is limited in maximum by the radius of the eclipsing cool giant. During transition to a quiescent phase it has to dilute or, at least, become to be optically thin, because the nebular emission dominates the near-UV/optical region (Fig. 11, see also [55]) and occupies a large volume in the binary. As a result the wave-like variation in the light curve develops (Fig. 11 top, also Figs. 3 and 4 of [55]).

Non-eclipsing systems: The system of AG Dra is seen more from its pole. Thus if the geometry of the material, which develops during outburst, is comparable to the eclipsing systems, the central ionizing source can be directly seen. As a result both a hot luminous blackbody and a strong nebular component of radiation are observed. The observed increase of the hot star luminosity at very high temperature produces a surplus of ionizing photons and thus leads to an additional extension of the HII zone (the parameter X increases, Sect. 2.2.2). In the case of an *open* ionized region ($X > 10$ for AG Dra parameters, cf. Fig. 3) a fraction of the ionizing photons escapes the system. Therefore an injection of new particles (emitters) into such the zone, for example in a form of the hot star wind, will produce an extra flux of the nebular nature. In the case of very fast wind one can expect an additional ionization due to collisions that explains the observed very high electron temperature during outbursts.

Creation of a disk-like structure around the hot star during outbursts could be qualitatively understood as a results of an expansion of the accretor's shell due to its fast rotation. In this case the hot components in symbiotic stars should rotate asynchronously with respect to the orbital motion. Contrary, in the case of a synchronous rotation, the ejected material will be spread into the space rather in form of a shell. This could be the case of BF Cyg, where only a blackbody component without any emission lines was observed in ultraviolet during its 1989 outburst (Fig. 7). The above mentioned effect of inclination can be additionally complicated by different properties of the mass outflow in different objects – mainly the rate, at which the material is being ejected – that may regulate its optical properties.

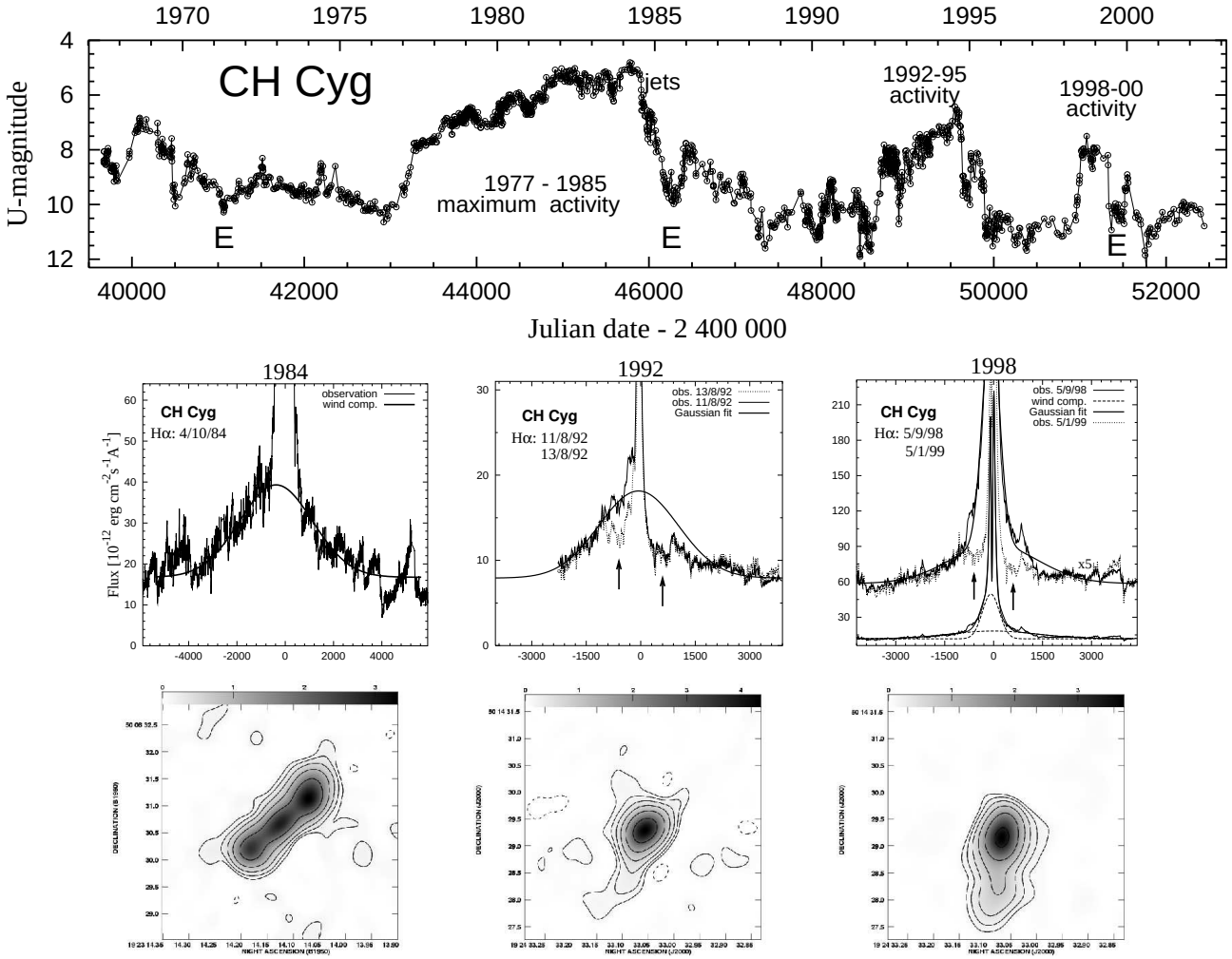

Figure 13: Top: The U-light curve of CH Cyg covering the period from 1967 to 2002.5. Middle: Hydrogen profiles during three active periods – in 1984 terminal velocities $v_\infty \approx 3\,500\,\mathrm{km\,s^{-1}}$. In the 1992-95 active phase $v_\infty \approx 3\,000\,\mathrm{km\,s^{-1}}$, and absorptions on both sides of the line profile at $\pm(400 - 600)\,\mathrm{km\,s^{-1}}$ appeared (marked by arrows). In the recent, 1998-00, activity basic signatures of the profiles were similar to those during the 1992-95. Solid thick lines represent the resulting fit by Gaussian functions. Broken lines are the broad components of the profile and denoted in panels as 'wind components'. Bottom: The remnants of the mass loss during activity after 1984.6 as detected by the VLA 5GHz radio maps on 1986, 1995 and 1999 (from left to right) [7].

However, this suggestion has to be confirmed by new multi-frequency observations of symbiotic stars during outbursts and theoretical modeling of the mass-loss to understand better physical processes responsible for outbursts of classical symbiotic systems. In the following section we propose a simple method to estimate the mass-loss rate from the Hα emission.

4.4 Mass loss in the symbiotic system CH Cyg

CH Cygni is a mysterious symbiotic star. It started a symbiotic activity in 1963. Prior to this, CH Cyg had been observed as a semi-regular variable (e.g.: [33]). Subsequently, the symbiotic phenomenon was observed during 1967-86, 1977-86, 1992-95 and 1998-00 (Fig. 13). Recent studies suggest that CH Cyg is an eclipsing triple-star system consisting of the inner, 756-day period binary (the symbiotic pair, which is responsible for the observed activity) and another cool giant revolving around it on the long, 14.5-year period orbit ([20,51,54], original suggestion of a triple-star model was set by [19]). The distance to CH Cyg was determined on the basis of Hipparcos measurements as 270 ± 66 pc (e.g.: [63]).

Active phases of CH Cyg after 1984.6 were characterized by pronounced signatures of a high-velocity mass outflow with terminal velocities of $2\,500 - 3\,500\,\mathrm{km\,s^{-1}}$. This and the vicinity of CH Cyg allowed us to obtain its spatially resolved images. For the first time [58] detected bipolar jets by the VLA radio observation. Further observations of the CH Cyg ejecta revealed a non-thermal emission at its outer parts and a precession with a period of ≈ 20 years [7,8]. A detail structure given by the ground-based observations and the HST was studied by [6,9]. Figure 13 shows some examples of the high-velocity features of CH Cyg.

The rate, at which the material is ejected by the central star, represents a very important parameter to understand a balance between the input and output of the energy during outbursts, ionization structure of the symbiotic nebulae, a mechanism of the mass-loss, etc. For symbiotic binaries an approximative approach to estimate the mass-loss rate for EG And, AG Peg and

AG Dra was used by [61,64,65]. In all cases the authors assumed an optically thin wind at a constant velocity ($v = v_\infty$). In the following section we introduce a simple Hα method to investigate the mass-loss rate during active phases of CH Cyg as recently suggested by [56].

4.4.1 Mass loss from the Hα emission

In the recombination process, the transition from the third to the second level of hydrogen has a high probability of producing the Hα line in emission. In the case of an ionized stellar wind, the Hα profile contains information on its emissivity and velocity distribution. Thus, having a theoretical Hα luminosity and some knowledge of the velocity field of the outflow, one can derive the mass-loss rate, $\dot{M}$, from the measured strength of the Hα emission. Here we use a simplified approach assuming that the wind is (i) spherically symmetric with a steady $\dot{M}$, (ii) fully ionized and completely optically thin in Hα from a radius $r_{\rm min}$ above the ionizing source and (iii) isothermal at the same temperature as the stellar photosphere. The total line luminosity, $L(\mathrm{H}\alpha)$, is related to the line emissivity of the wind, $\varepsilon_\alpha n_{\rm e} n^+$, by

$$L(\mathrm{H}\alpha) = 4\pi d^2 F(\mathrm{H}\alpha) = \varepsilon_\alpha \int_V n_{\rm e} n^+(r)[1 - w(r)]\,\mathrm{d}V, \quad (16)$$

where d is the distance to the system, $F(\mathrm{H}\alpha)$ represents the observed flux in Hα (erg cm^{-2} s^{-1}), ε_α is the volume emission coefficient in Hα, $n_{\rm e}$ and n^+ are number densities of electrons and ions (protons) and the factor $w(r)$ is the fraction of the solid angle that is covered by the photosphere (so called geometrical dilution factor). Further assumption of a constant value of $\varepsilon_\alpha = 3.56 \times 10^{-25}$erg cm^3 s^{-1} throughout the ionized medium at the electron temperature of $T_{\rm e}$ = 10^4 K simplifies considerably the approach. For a completely ionized medium, ($n_{\rm e} \simeq n^+$), the particle density $n(r)$ in the wind can be expressed in terms of the mass-loss rate and the velocity law via the mass continuity equation as

$$n(r) = \dot{M}/4\pi r^2 \mu m_{\rm H} v(r), \quad (17)$$

where μ is the mean molecular weight, $m_{\rm H}$ is the mass of the hydrogen atom and $v(r)$ is the velocity distribution in the hot star wind, approximation of which is given by Eq. 5. According to these assumptions, [56] derived an expression for the Hα luminosity as

$$L(\mathrm{H}\alpha) = \frac{\varepsilon_\alpha}{4\pi(\mu m_{\rm H})^2} \Big(\frac{\dot{M}}{v_\infty}\Big)^2 \frac{1}{R_\star} \times I_{\rm w}, \quad (18)$$

where the integral $I_{\rm w}$ is a function of the γ and $r_{\rm min}$ parameters (see [56] for more detail). Then comparing the observed Hα luminosity from the wind with Eq. 18, one can obtain the mass-loss rate. [56] estimated the γ parameter by comparing a synthetic-line profile to the observed one. They obtained average values of γ = 1.4 and 1.9 for 1984.6-92 and 1998-00 active phases, respectively. For other input quantities, the radius of the active star in CH Cyg $R_\star = 5\,\mathrm{R}_\odot$, $r_{\rm min} = 8 - 9\,\mathrm{R}_\odot$ and the outer radius of 200 R$_\odot$ (= a finite limit, at which the wind contributions are negligible), they determined the mass-loss rate from the active star

$$\begin{aligned} \dot{M}_{1984} &= (4.4 \pm 1.5) \times 10^{-6} \mathrm{M}_\odot\,\mathrm{yr}^{-1} \\ \dot{M}_{1998} &= (1.8 \pm 0.7) \times 10^{-6} \mathrm{M}_\odot\,\mathrm{yr}^{-1}. \end{aligned} \quad (19)$$

These values correspond to the measured Hα fluxes converted to the scale of luminosities for the distance of 270 pc. It is important that our $\dot{M}$ estimates agree well with mass-loss rates derived from radio observations [52,58]. The radio mass-loss rates are less model dependent than the Hα method. In the former case we observe the ejected material at very large distances from the star (from a few 10's of A.U. to $\approx$1 000 A.U.), where a constant expansion velocity can be reliably assumed. On the other hand, in the latter approach we are dealing with regions at distances of a few R$_\odot$ to, at maximum, a few hundreds of R$_\odot$, the emissivity of which critically depends on the velocity law, whose structure, however, has to be assumed.

5 Conclusions

Symbiotic stars represent very suitable space laboratories for studying processes of ionization and recombination. This paper reviewed some recently investigated effects of these processes. It was found that the ionization structure of symbiotic nebulae can be very different and variable during different levels of activity and thus can significantly influence our observations.

During *quiescent* phases, when the compact hot star produces the energy at approximately the same amount and temperature, an effect mimicking the reflection effect takes place. It was found that the observed total emission from the symbiotic nebula is consistent with that given by a simple ionization model and the variation in the emission measure is fully responsible for variation observed in the light curves. To explain the orbitally-related variation, it is assumed that the nebula is partially optically thick and of a non-symmetrical shape. Future work should thus include investigation of the optical properties of symbiotic nebulae. First, under conditions of a simple ionization model, with further implementation of effects of the wind accretion onto the compact object. The latter is closely connected with 2D and 3D hydrodynamical calculations of gas flow in symbiotic stars to model a more realistic density distribution (e.g.: [16,67]). Also this is important to continue the long-term photometric monitoring of well studied symbiotic stars to obtain information on the geometry and location of the optically thick portion of the symbiotic nebula in the system. An extension of such the monitoring programme to the near-IR region is desirable to search for a double-wave variability in the VRI bands to test the possibility of an ellipsoidal shape of red giants in symbiotic binaries.

During *transition* periods – from activity to quiescence – a gradual variation in the luminosity of photons capable ionizing hydrogen results in a systematic variation in the structure of the HII region. As the symbiotic nebulae are not symmetrically placed around the binary axis, their gradual change in the geometry and location in the binary can produce the observed variation in the $O - C$ residuals and thus an apparent change in the period. This effect is best indicated for eclipsing systems.

During *active* phases the ionization structure of symbiotic nebulae is disrupted by the mass flow from the active star. The result depends on the mass outflow properties and the binary parameters – mainly the orbital inclination. By disentangling the observed SED for the example objects, it was found that in the non-eclipsing systems (e.g. AG Dra) the nebular component of radiation in the continuum considerably strengthened at a

high electron temperature of about 30 000 K. On the other hand, eclipsing systems (e.g. CI Cyg) display simultaneous presence of a cool pseudophotosphere with the superposed highly ionized lines in the ultraviolet. This suggests an optically thick disk-like torus encompassing the hot star and being coincident with the orbital plane. The nebular contribution in the continuum here is very faint and corresponds to a low electron temperature of $\sim$8 000 K. To understand better the mechanism of the mass ejection, multi-frequency observations of symbiotic stars during outbursts and theoretical modeling of the mass outflow are highly desirable. Example of an improved method to estimate the mass-loss rate during active phases of CH Cyg suggested values of $\dot{M} = (1.8 - 4.4) \times 10^{-6} \mathrm{M}_{\odot}\,\mathrm{yr}^{-1}$. We propose to apply, at least, this approach to other systems with significant features of a high-velocity mass outflow.

Acknowledgments. A part of this research has been done within the project No. SLA/1039115 of the Alexander von Humboldt foundation during the author's visits at the Astronomical Institute in Bamberg, in part throughout the bilateral research project between the Royal Society of Great Britain and the Slovak Academy of Sciences and also was partly supported by the Slovak Academy of Sciences grant No. 1157 and by the APVT-20-014402 Project.

References

[1] Belyakina, T.S. 1965, Izv. Krymsk. Astrofiz. Obs. 33, 226

[2] Belyakina, T.S. 1970a, Izv. Krymsk. Astrofiz. Obs. 41-42, 275

[3] Belyakina, T.S. 1970b, Astrofizika 6, 49

[4] Belyakina, T.S. 1985, IBVS No. 2698

[5] Boyarchuck, A.A. 1966, Astron. Zh. 43, 976

[6] Corradi, R.L.M., Munari, U., Livio, M., Mampaso, A., Goncalves, D.R., Schwarz, H.E. 2001, ApJ 560, 912

[7] Crocker, M.M., Davis, R.J., Eyres, S.P.S., Bode, M.F., Taylor, A.R., Skopal, A., Kenny, H.T. 2001, MNRAS 326, 781

[8] Crocker, M.M., Davis, R.J., Eyres, S.P.S., Bode, M.F., Skopal, A. 2002, MNRAS (in press)

[9] Eyres, S.P.S., Bode, M.F., Skopal, A., Crocker, M.M., Davis, R.J., Taylor, A.R. 2002, MNRAS (in press)

[10] Fekel, F.C., Hinkle, K.H., Joyce, R.R., Skrutskie, M.F. 2001, AJ 121, 2219

[11] Fernández-Castro, T., Cassatella, A., Giménez, A., Viotti, R. 1988, ApJ 324, 1016

[12] Fernie, J.D. 1985, PASP 97, 653

[13] Fleming, W.P. 1912, Ann. Harv. Coll. Obs. 56, 165

[14] Folini, D., Walder, R. 2000, Ap&SS 274, 189

[15] Gális, R., Hric, L., Friedjung, M., Petrík, K. 1999, A&A 348, 533

[16] Gawryszczak, A.J., Mikolajewska, J., Rózyczka, M. 2002, A&A 385, 205

[17] González-Riestra, R., Viotti, R., Iijima, T., Greiner, J. 1999, A&A 347, 478

[18] Greiner, J., Bickert, K., Luthardt, R., Viotti, R., Altamore, A., González-Riestra, R., Stencel, R.E. 1997, A&A 322, 576

[19] Hinkle, K.H, Fekel, F.C., Johnson, D.S., Scharlach, W.W.G. 1993, AJ 105, 1074

[20] Iijima, T. 1998, MNRAS 297, 77

[21] Hric, L., Skopal, A., Urban, Z., Komžík, R., Luthardt, R., Papoušek, J., Hanžl, D., Blanco, C., Niarchos, P., Velič, Z., Schweitzer, E. 1993, Contr. Astron. Obs. Skalnaté Pleso 23, 73

[22] Jacchia, L. 1941, Bull. Harv. Coll. Obs. No. 915

[23] Kenyon, S.J. 1986, The symbiotic stars, Cambridge Univ. Press, Cambridge, p. 27

[24] Kenyon, S.J., Oliversen, N.A., Mikolajewska, J., Mikolajewski, M., Stencel, R.E., Garcia, M.R., Anderson, C.M. 1991, AJ 101, 637

[25] Kenyon, S.J., Mikolajewska, J., Mikolajewski, M., Polidan, R.S., Slovak, M.H. 1993, AJ 106, 1573

[26] Luthardt, R. 1984, IBVS No. 2495

[27] Luthardt, R. 1989, Veroff. Sterne Sonneberg 10, 255

[28] Meinunger, L. 1983, Mitt. Verand. Sterne 9, 92

[29] Merrill, P.W. 1941, PASP 53, 121

[30] Merril, P.W., Humason, M.C. 1932, PASP 44, 56

[31] Mikolajewska, J., Kenyon, S.J., Mikolajewski, M. 1989, AJ 98, 1427

[32] Mikolajewska, J., Kenyon, S.J., Mikolajewski, M., Garcia, M.R., Polidan, R.S. 1995, AJ 109, 1289

[33] Mikolajewski, M., Mikolajewska, J., Khudyakova T.N. 1990, A&A 234, 219

[34] Munari, U. 1989, A&A 208, 63

[35] Mürset, U., Schmid, H.M. 1999, A&ASS 137, 473

[36] Nussbaumer, H., Vogel, M. 1987, A&A 182, 51

[37] Ogley, R.N., Chaty, S., Crocker, M., Eyres, S.P.S., Kenworthy, M.A., Richards, A.M.S., Rodríguez, L.F., Stirling, A.M. 2002, MNRAS 330, 772

[38] Pereira, C.B., Landaberry, S.J.C. 1996, AJ 111, 1329

[39] Proga, D., Kenyon, S.J., Raymond, C., Mikolajewska, J. 1996, ApJ 471, 930

[40] Proga, D., Kenyon, S.J., Raymond, C. 1998, ApJ 501, 339

[41] Schild, H., Schmid, H.M. 1996, A&A 310, 211

[42] Schmid, H.M. 1998, Rev. in Mod. Astronomy 11, p. 297

[43] Schmid, H.M., Schild H. 1997, A&A 321, 791

[44] Schmutz, W., Schild, H., Mürset, U., Schmid, H.M. 1994, A&A 288, 819

[45] Seaquist, E.R., Taylor, A.R., Button, S. 1984, ApJ 284, 202

[46] Skopal, A. 1994, IBVS No. 4096

[47] Skopal, A. 1996, Ap&SS 238, 285

[48] Skopal, A. 1998, A&A 338, 599

[49] Skopal, A. 2001, Contrib. Astr. Obs. Skalnate Pleso 31, 119

[50] Skopal, A. 2001, A&A 366, 157

[51] Skopal, A., Bode, M.F., Lloyd, H.M., Tamura, S. 1996, A&A 308, L9

[52] Skopal, A., Bode, M.F., Bryce, M., Chochol, D., Davis, R.J., Errico, L., Evans, A., Eyres, S.P.S., Hric, L., Ivison, R.J., Kenny, H.T., Komžík, R., Meaburn, J., Tamura S., Taylor, A.R., Urban, Z., Vittone, A.A. 1996, MNRAS 282, 327

[53] Skopal, A., Vittone, A., Errico, L., Bode, M.F., Lloyd, H.M., Tamura, S. 1997, MNRAS 292, 703

[54] Skopal, A., Bode, M.F., Lloyd, H.M., Drechsel, H. 1998, A&A 331, 224

[55] Skopal, A., Teodorani, M., Errico, L., Vittone, A., Ikeda, Y., Tamura, S. 2001, A&A 367, 199

[56] Skopal, A., Bode, M.F., Crocker, M.M., Drechsel, H., Eyres, S.P.S., Komžík, R. 2002, MNRAS (in press)

[57] Skopal, A., Baluďanský, D., 2003, In: Corradi, R.M.L. Mikolajewska, J. (Editors), Symbiotic stars probing stellar evolution, ASP Conf. Ser. (in press)

[58] Taylor, A.R., Seaquist, E.R., Mattei, J.A. 1986, Nat. 319, 38

[59] Tomov, N.A., Tomova, M.T., Ivanova, A. 2000, A&A 364, 557

[60] Tomov, N.A., Tomova, M.T. 2002, A&A 388, 202

[61] Tomova, M.T., Tomov, N.A. 1999, A&A 346, 151

[62] Viotti, R. 1994, IAU Circ. No. 6044

[63] Viotti, R., Badiali, M., Cardini, D., Emanuele, A., Iijima, T. 1997, In: B. Batrick (Editor), *Hipparcos* Venice 1997, ESA-SP-402, Esa Publ., Nordwijk, p. 405

[64] Vogel, M. 1993, A&A 274, L21

[65] Vogel, M., Nussbaumer, H. 1994, A&A 284, 145

[66] Walder, R. 1995, In: van der Hucht, K.A., Williams, P.M. (Editors), Wolf-Rayet Stars: Binaries, Collidings Winds, Evolution., IAU Symp. 163, p. 420

[67] Walder, R., Folini, D., 2000, In: H.J.G.L.M. Lamers, A. Sapar (Editors), Thermal and Ionization Aspects of Flows from Hot Stars., ASP Conf. Ser. Vol. 204, p. 331